CORE
Metadata, citation and similar papers at core.ac.uk
Provided by LJMU Research Online

A test-proven As-grown-Generation (A-G) model for predicting NBTI under use-bias

Z. Ji (z.ji@ljmu.ac.uk), J. F. Zhang, L. Lin, M. Duan, W. Zhang, X. Zhang, R. Gao, B. Kaczer(1), J. Franco(1), T. Schram(1), N. Horiguchi(1), S. De Gendt(1), and G. Groeseneken(1)
School of Engineering, Liverpool John Moores University, Liverpool L3 3AF, UK. (1)IMEC, Leuven B3001, Belgium

Introduction: The gap between modelling and real performance has been identified as a major constraint for design optimisation [1] and the inaccuracy of NBTI models contributes to it. When developing a NBTI model, short-term accelerated tests are usually used to extract model parameters and it is a common practice to 'qualify' a model by showing it fits well with test data. The models 'qualified' in this way, such as the reaction-diffusion (R-D) framework [2], cannot predict the long-term NBTI under low use-bias for both SiON and HKMG processes (**Figs.1a&b**). *There is a pressing need for delivering the original mission: reliably predicting long term NBTI at low use-bias, based on a model extracted from Vg-accelerated short tests.*

Key advance of this work: The As-grown-Generation (A-G) model [3] has successfully demonstrated its excellent predicting capability on device reliability and variability under DC NBTI [4] and HCI conditions [5]. *This work demonstrates, for the first time, (i) both DC and AC NBTI under use-overdrive Vg_ov can be reliably predicted from the A-G model extracted from Vg-accelerated short tests (**Figs.1c-d**), and (ii) the same model can also predict the NBTI under variable operational workload (**Fig.2**), needed for dynamic voltage scaling power management [6].* The model needs only three fitting parameters. We emphasize that the A-G model is extracted from the accelerated short DC tests and the test data at low biases in lower panels of **Fig.1c&d** were not used for fitting. This success is achieved after a detailed understanding of different types of defects and their contributions to NBTI, based on direct measurements of each type of defects (**Table I**) , as described below.

Measuring different types of defects: Devices from three different processes are used, including HKMG and SiON (**Table II**). Measurement with 3µs speed is used for both DC&AC NBTI under 125 °C. Early works [3] reported that as-grown hole trap (AHT) and generated defects (GD) are located below and above the energy level E(VgGD) (**Fig.3**) respectively, allowing their separation. For unipolar AC stress, the defects above E(Vg=0V) do not discharge once generated, but those between E(VgGD) and E(Vg=0) do. As a result, the GDs are further separated into two parts: the anti-neutralization positive charges (ANPC) above E(Vg=0V) and the cyclic positive charges (CPC) between E(VgGD) and E(Vg=0V) (**Fig.3**).

The Vg waveform for their measurement under DC and AC stress is given in **Figs.4a&d,** respectively. '☆' in **Fig.4b** is the sum of all defects. By biasing at VgGD (**Fig. 3**), all AHTs are discharged, so that AHT ('Δ' in **Fig.4c**)='☆'-'**x**'. The device was then biased at Vg=0V to discharge CPC, so that CPC ('◁' in **Fig.4c**)='**x**'-'◊' and ANPC='◊' (**Figs.4c**). For AC stress, total ΔVth are measured on two edges: one from zero to Vgst ('**o**') as "End-of-Recovery (EoR)" and the other from the opposite edge ('□') as "End-of-Stress (EoS)" (**Figs.4d&e**). This gives two sets of AHTs in **Fig.4f**: AHT_EoS ('Δ')='□'-' **x**' and AHT_EoR('▽')= '**o**'-' **x**'. The CPC and ANPC were evaluated in the same way as that after DC stress. Their properties and contributions to NBTI are examined next.

Anti-neutralization positive charges (ANPC): For the same effective stress time, the same ANPC was obtained for DC and AC stresses at different frequencies (**Fig.5a**), as ANPC does not neutralize during AC stress. ANPC generation follows power law against both stress time (**Fig.5b**) and stress Vgst_ov (**Fig.5c**) and the exponents are independent of Vg and stress time, laying the foundation for reliable prediction. ANPC are modelled with three fitting parameters: g_0, m, n (**eq.1, Table I.)**

As-grown hole traps (AHT): Under DC stress, more AHTs are charged at higher |Vg| (**Figs.6a&b**), but the normalized kinetics is the same (**Fig.6c**). Under AC stress, AHT_EoS reduces for higher frequency (**Fig.7a**), because of shorter charging time, tch=period/2. With the same tch, AHT_EoS agrees well with AHT_DC (**Fig.7c**). Charging AHTs can be fully modelled by the kinetics (**Fig.6c**) with its saturation level taken from **Fig.6b**. The efficient discharging under Vg leads to AHT_EoR≈0 for all frequencies (**Fig.7b**). This explains AHT_EoS=AHT_DC for the same tch, since charging restarts from ~zero in each cycle. The discharge kinetics is independent of |Vgst_ov| (**Fig.8a&b**) and used for modelling discharge.

Cyclic positive charges (CPC): CPC is the same for DC and AC initially (<50sec, **Fig.9a**), but CPC_DC saturates at a higher level eventually. To understand this, CPC_DC was neutralized and recharged (**Fig.9b**). CPC can be filled to saturation much faster in the recharging compared with 1st DC stress, confirming they are generated defects. Moreover, these generated CPC clearly has two components: i) fast-charging CPC (fCPC) recharged fully within 1µs, and ii) slow-charging CPC (sCPC) only starts recharging after 5ms and reach saturation after 10s. Their different dependence on stress Vg in **Fig.10a** supports that they are different defects. For DC NBTI, sCPC charging is modelled by the kinetics in **Fig.9b**. For AC NBTI, sCPC contributes little to charging (**Fig.9a**) as total CPC_AC=fCPC, because discharging is far more efficient than charging (**Fig.10b V.S. Fig.9b**). There is no need to model sCPC for AC NBTI, therefore. In contrast, charging fCPC is far more efficient than discharging (**Fig.9b V.S. Fig.10c**) and contributes to AC NBTI. Similar to AHTs, fCPC is modelled by the saturation level in **Fig.10a** and the discharging kinetics in **Fig.10c**.

Aging Prediction: Four Vg-accelerated short (1ks) DC stresses (**Fig.1c**) were carried out to extract the A-G model (**Table I**), giving 3 fitted parameters in **Table II**. The model can successfully predict both DC and AC NBTI under use-Vg_ov (**Figs.1c&d**), delivering the original mission of NBTI modelling. The NBTI under variable operation Vg_ov is also successfully predicted (**Fig.2**). Moreover, the A-G model predicts the frequency (Freq) and duty-factor (DF) dependence under operation condition well (**Figs.11a&b**). The contributions of different defects are also shown in **Figs.11a&b**. AHT is mainly responsible for the Freq- and DF-dependence of ΔVth_EoS. A higher Freq or smaller DF reduces the charge time at 'End-of-Stress' and in turn fills less AHTs (**Fig.7sa&b**). At 'End-of-Recovery', however, AHTs≈0 for all frequencies due to efficient discharging (**Fig.7b**), resulting in the well-known frequency-independence of NBTI [7]. Over 1MHz, AHT≈0 and ΔVth_EoS=ΔVth_EoR. Both ANPC and fCPC are frequency independent.

Process independence: The A-G model was applied to two other processes to prove it is not process specific. The measured Freq- and DF-characteristics under low Vg_ov agree well again (**Figs.12a-d**) with the predicted ones using A-G model extracted from the short DC stresses at high biases, in **Table II**.

An analysis of the success: To understand why A-G model can predict and early models [2] cannot, it is realized that the charging or generation of some defects will saturate with time during aging, like AHTs (**Fig.6c**) and CPCs (**Figs.9b**). However, ANPC does not saturate (**Fig.5**) and thus controls the long term aging. The A-G model's success comes from its accurate separation of ANPC from the rest of defects, enabling the reliable prediction from accelerated Vg to use Vg_ov. Only one non-saturating aging kinetic is needed: a power law with Vg- and time-independent exponents for ANPC (**Fig.5**). The R-D framework [2] has to use two separate non-saturating kinetics with more fitting parameters, because the real non-saturating component was not properly separated out. The contamination of non-saturating defects by the saturated ones results in erroneous power exponents and prediction.

Conclusions: For the first time, we demonstrate that A-G model extracted from short Vg-accelerated stresses can predict both long term DC and AC NBTI under low and dynamic operation Vg. This is achieved by successfully separating non-saturating defects from the saturating ones, allowing reliable extraction of power exponents needed for long term prediction. Unlike R-D model, A-G model does not require solving differential equations for AC NBTI. This saves computation time significantly, especially for high-frequency that needs small time-step, and makes it readily implementable in SPICE-like simulators.

Acknowledgement: This work is supported by EPSRC of UK (EP/L010607/1).
[1] G. Yeap, IEDM, 2013. **[2]** S. Desai, et al, IRPS 2013. **[3]** Z. Ji, et al, IEDM, 2013. **[4]** M. Duan, et al, VLSI, 2014. **[5]** M. Duan, et al, submitted to VLSI, 2015. **[6]** P. Mercati et al, DAC, 2013. **[7]** R. Fernandez, et al, IEDM, 2006.

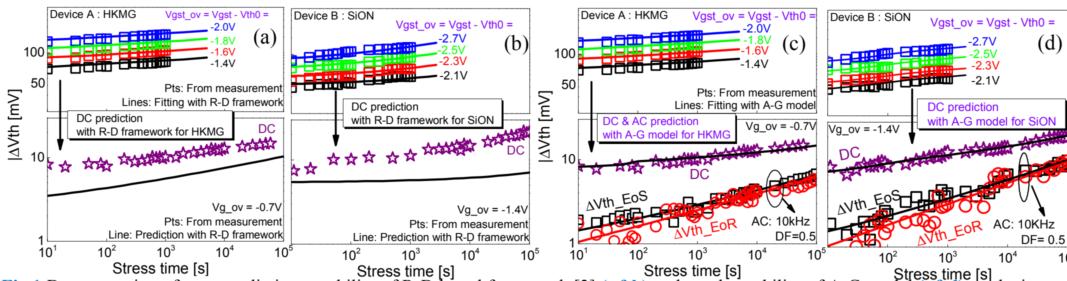

Fig.1 Demonstration of poor predictive capability of R-D based framework [2] **(a&b)** and good capability of A-G model **(c&d)** on devices with HKMG and SiON gate stack. Symbols are test data and lines are calculated. The SAME four Vg-accelerated short DC stresses were used to extract model parameters for both R-D and A-G models (HKMG: **a&c**; SiON: **b&d**). The accelerated data can be fitted well by both models (the upper panels of **a-d**). The extracted R-D model, however, cannot predict the ΔVth under low use-Vg_ov, as shown by the difference between symbols and lines in the lower panels of **a&b**). In contrast, the extracted A-G model predicts well not only for DC, but also for AC, NBTI under the SAME low use-Vg_ov (the lower panels of **c&d**). The test data in the lower panels of **a-d** were not used for fitting.

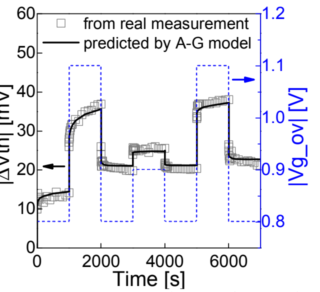

Fig.2 Demonstration of good predictive capability of A-G model on reliably predicting degradation under dynamic workload. Process-A is used.

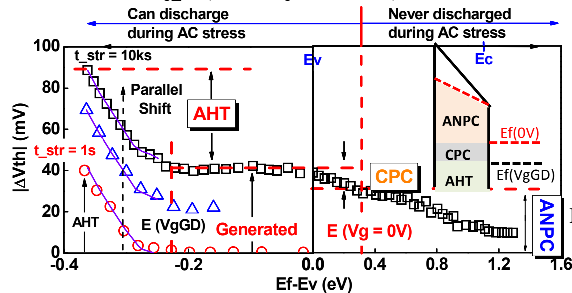

Fig.3 Defects separation based on their energy location. As-grown hole traps (AHT) are below E(VgGD) and the generated defects (GD) are above E(VgGD). GD is further separated into CPC between E(VgGD) and E(Vg=0V) and ANPC above E(Vg=0). For unipolar AC, ANPC never discharges. The energy location of each defect is illustrated in the inset.

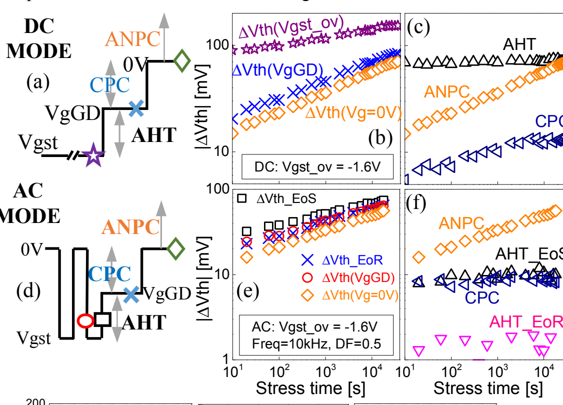

Fig.4 Defect separation under DC **(a-c)** and AC **(d-f)** stresses. For DC, ΔVth is recorded before (□) and after discharging under VgGD (×) and 0V (◊). For AC, ΔVth is monitored at two edges: from 0V to Vgst_ov – End of Recovery (EoR, o) and the following edge from Vgst_ov – End of Stress (EoS, □). The separation of three components (AHT, CPC and ANPC) for DC is by: AHT: Δ=□-x, CPC: ◁=x-◊, and ANPC=◊. For AC, AHT_EoS: Δ=a-x and AHT_EoR: ▽= O-x.

Table I. Components and Equation used for A-G model

$$\Delta Vth = ANPC + AHT + CPC,\quad CPC = fCPC + sCPC$$

Only ANPC is modeled by fitting **Fig. 5** with equation of 3 parameters: g_0,m,n

$ANPC = g_0 * Vgov^m * t^n$ (1)

The maganitude and charging/discharging kinetics of AHT, fCPC, sCPC is extracted directly from experiments (**Fig.6 - Fig.10**).

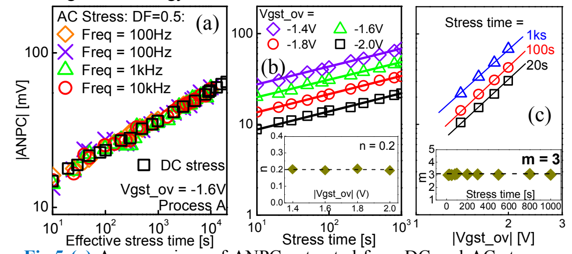

Fig.5 (a) A comparison of ANPC extracted from DC and AC stress. ANPC_DC agrees with ANPC_AC that is frequency-independent. **(b)** The generation kinetics of ANPC. The time exponent is independent of Vgst_ov (inset). **(c)** ANPC for a given stress time follows a power law against Vgst_ov and the voltage exponent is independent of time (inset).

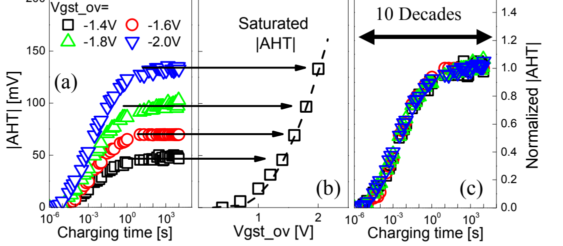

Fig.6 (a) AHT_DC kinetics under different Vgst_ov. It saturates in short time. **(b)** The experimentally measured saturation level under different Vgst_ov. The dash line is a guard to the eye. **(c)** When AHT_DC is normalized against its saturation value, it follows the same charging kinetics.

Table II Devices used in the work and the extracted model parameters

ID	Device	g_0	m	n
A	EOT=1.43nm HKMG Al2O3 capping	1.75E-03	3	0.2
B	EOT = 1.0nm HKMG	4.90E-03	3.38	0.22
C	EOT=2.3nm plasma-N SiON	1.00E-04	4.49	0.25

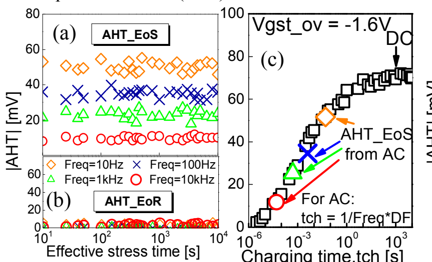

Fig.7 AHT at the end of AC stress (EoS) edge and end-of-recovery (EoR) edge. **(a)** AHT_EoS reduces for higher frequency. AHT_EoR is negligible for all frequencies. **(b)** For the same charging time, tch=period*DF (duty factor) for AC, AHT_EoS agrees with AHT_DC.

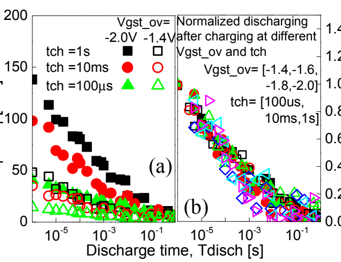

Fig.8 (a) AHT discharge kinetics and **(b)** the normalization under different Vgst_ov or charging time, tch. The kinetics is independent of Vgst_ov and tch.

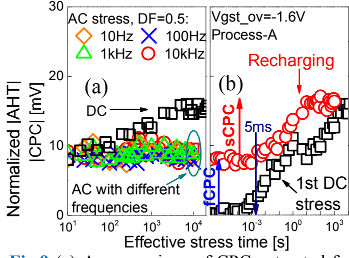

Fig.9 (a) A comparison of CPC extracted from DC and AC stress. Within 50s, CPC_DC ≈ CPC_AC regardless of frequency. For longer stress time, CPC saturates and CPC_DC > CPC_AC. (b) A comparison of CPC_DC under the 1st stress and recharge. CPCs were fully discharged before recharge. Some CPCs were filled within 1μs (fCPC), whilst the rest only starts filling after 5ms (sCPC). Total AC CPC in (a) agrees well with the fCPC in (b).

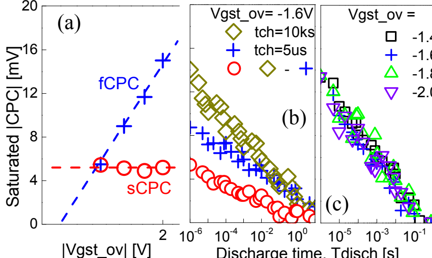

Fig.10 (a) The saturated fCPC and sCPC have different dependence on Vgst_ov. The extraction procedure is shown in Fig.9(b). **(b)** fCPC discharge kinetics ('+') is obtained by discharging after only 5μs recharging on a stressed device. The sCPC discharge kinetics ('o') is obtained by subtracting fCPC from the total CPC ('◊'). **(c)** Normalized fCPC discharge kinetics is independent of Vgst_ov.

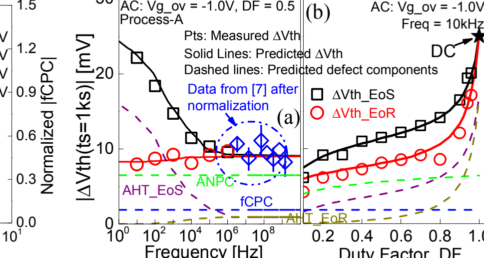

Fig.11 A comparison of the measured (symbols) and predicted (solid lines) Frequency **(a)** and Duty Factor **(b)** characteristics of AC-aging under low operating condition for process A. The detailed contribution of each type of defects are shown in dashed lines.

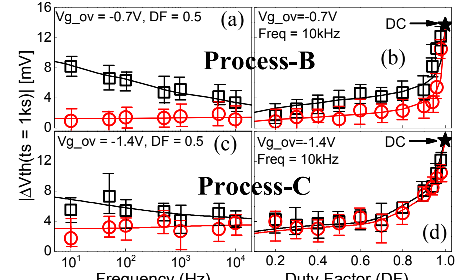

Fig.12 A comparison of the measured (symbols) and predicted (lines) Frequency **(a&c)** and Duty Factor **(b-d)** characteristics of AC-aging under lowest possible Vg for process B&C. To improve the measurement accuracy, four samples are used for each stress condition and then averaged value is used.